ORIGINAL ARTICLE

Phased array calibration system with high accuracy and low complexity

Sol Kim [a], Hyun-Jun Dong [b], Jong-Won Yu [a], Han Lim Lee [b],*

[a] *School of Electrical Engineering, Korea Advanced Institute of Science and Technology (KAIST), Daejeon 34141, South Korea*
[b] *School of Electrical and Electronics Engineering, Chung-Ang University, Seoul 06974, South Korea*

Abstract This paper presents a highly efficient phased array calibration system for phase and magnitude error correction. The proposed calibration system is based on far-field scanning of the array antenna under test at factory level. Since the proposed structure requires a magnitude detection only for vector calibration, low circuit complexity can be achieved. Unlike the conventional far-field calibration based on rotating-element electric-field vector (REV) method to find maximum vector-sum point, the proposed system detects the minimum vector-sum point and tracks the behavior of the null point. To verify the feasibility of the proposed system for large-scale array antenna, 4×4 phased array antenna is implemented at 5.8 GHz. Then, the proposed method is applied to the phased array antenna and compared with the conventional REV method.

1. Introduction

Phased array antennas (PAAs) play a very important role in modern radar [1–6], satellite [7,8], and future 5G communication systems [9–12]. Since the expected antenna elements in the PAAs increase as the frequency band for the next generation sensor and communication moves higher, RF synchronization for multiple beamforming chips is considered as the key technique for future PAA applications. However, the phase and amplitude errors always come with the initial integration of

large-scale PAAs and consequently cause the radiation pattern distortion and degradation in the overall system performance [13,14]. Therefore, vector calibration for PAAs should be required at least in a production verification level so that the potential errors can be compensated before operation. Since there have been many different calibration methods for PAAs, typical calibration techniques are first compared as shown in Fig. 1. A calibration line method that compares the signals coupled from each RF chain [4,5,15] is shown in Fig. 1 (a). Although this method allows self-calibration by the embedded lines, the increase in the required number of coupled lines and potential error by the coupled line itself make it impractical for large-scale PAA. Also, the peripheral fixed probe method uses the probe inserted between antennas to compensate for errors as shown in Fig. 1 (b) [6,15–17]. However, the size of the PAA increases due to the probe inserted into the array antennas. Then, the mutual coupling method can be also considered to
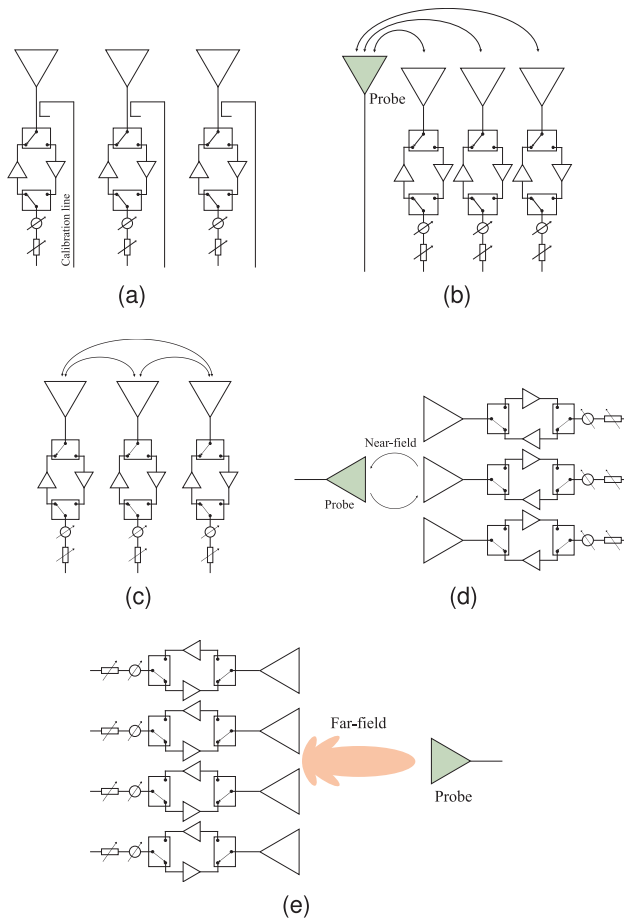
Fig. 1 Various calibration methods for the PAA with (a) calibration line, (b) peripheral fixed probe, (c) mutual coupling, (d) near-field probe, and (e) far-field probe.

compare signals without adding extra antennas or increasing array sizes as shown in Fig. 1 (c) [15,18–22]. But, in non-uniform arrangement of antenna elements, this method requires a complex calibration algorithm, resulting in lowering calibration accuracy.

Unless a real-time onboard calibration is necessary, the calibration method based on the look-up table (LUT) generated by an initial calibration at manufacturing level might be sufficient. Then, the near-field probe method and the far-field scanning method can be considered for generating the initial calibration LUT for large-scale PAAs. Fig. 1 (d) shows the near-field probe method [6,15,17]. In this method, the near-field probe antenna detects the amplitude and phase of each individual element of the PAA through mechanical movement. However, as array antenna size increases, the time required for calibration increases drastically due to the mechanical movement of the probe over the whole array. On the other hand, the far-field calibration method as shown in Fig. 1 (e) measures the combined electric field vector of the PAA by the referece antenna in the far-field region to calibrate for the magnitude and phase of each element [23–26]. This method can easily

calibrate the amplitude and phase of each element by only measuring the received power. One of the most popular methods based on this far-field calibration is the rotating-element electric-field vectors (REV) technique [23–29]. The REV method rotates the phase of each antenna element in the PAA from 0° to 360° and finds a maximum level of all combined electric field vectors as shown in Fig. 2 (a). However, the problem with the REV method is the small dynamic range with respect to the change in phase around the maximum received power. In [26], Composite power curves according to phase change of REV method are expressed using theoretical and measured values. The small dynamic range of the REV method is also observed. That is, the system cannot find the correct phase calibration values due to a small power resolution near the maximum point of combined electric field vectors, which causes the calibration error. A calibration method in the initial factory level aims to have high accuracy.
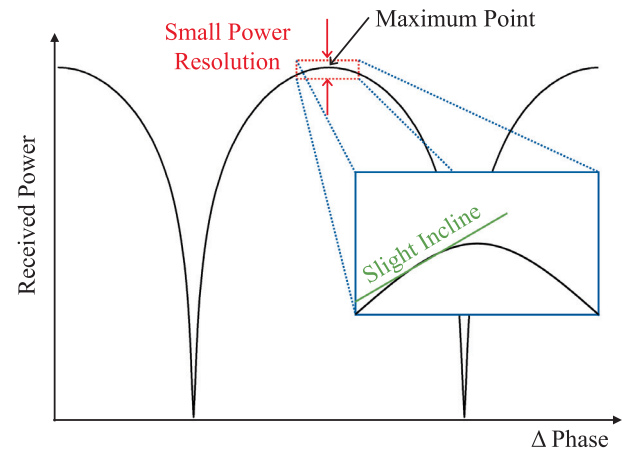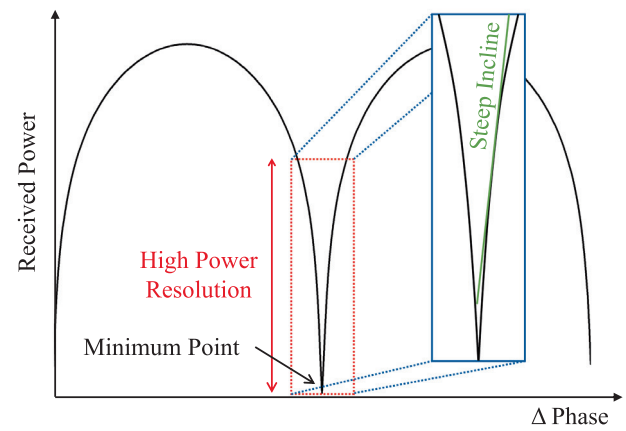
Fig. 2 Received power by combined electric field of (a) conventional REV method and (b) proposed method.

Because we want PAAs with good performance without error when PAAs are mass-produced at the factory. Therefore, this paper proposes a new calibration method to solve the problems of the conventional REV method. Unlike the REV method, the proposed method tracks the minimum level of the far-field received power to increase the dynamic range per phase change as shown in Fig. 2 (b). Since the changes in the received power level can be more accurately read due to the high dynamic range near the null, higher calibration resolution per phase adjustment can be achieved. That is, Fig. 2 shows the calibration resolution, which is "power change/phase error", for finely discriminating phase errors to compare the power change according to the phase change near the maximum and minimum power. The configuration of this paper is as follows. In Section 2, theoretical analysis and the simulation of the proposed method are presented. In Section 3 and 4, the proposed calibration system is designed and verified with the 4×4 PAA fabrication and measurement. Then, the proposed method is compared with the conventional REV method. Lastly, the conclusion of this work is given in Section 5.

2. Proposed method theory and simulation

2.1. Theory of proposed method

The concept of the proposed method is based on the array factor equations. Fig. 3 (a) shows a diagram to describe the array factor of the PAA. Each antenna element is linearly arranged on the z-axis, and a uniform plane wave arrives at all of the elements with an angle of incidence (θ). The phase difference of each element is then generated with ψ. N is the total number of antenna elements in the array, and ω_n is a n-th weighted vector. d is the distance between the antennas. Assuming a uniform linear array has $\omega_n = 1$, then the array factor is given by (1). It can be presented simply as follows (2), where k is the wave number, and can be expressed as (3) by normalization.

$$AF = 1 + e^{j\psi} + e^{j2\psi} + \cdots + e^{j(n-1)\psi} + \cdots + e^{j(N-1)\psi} \qquad (1)$$

$$AF = e^{jk(N-1)\psi/2} \frac{sin(N\psi/2)}{sin(\psi/2)} \qquad (2)$$

$$AF_N = \frac{sin(N\psi/2)}{Nsin(\psi/2)} \qquad (3)$$

Assuming $N = 2$, and $d = \lambda/2$, Fig. 3 (b) shows the array factor according to the phase difference (ψ) between the two antennas, and the location of the null according to the angle of incidence (θ). When the angle of incidence is 90°, broadside, the null occurs at 180° of phase difference. Fig. 3 (c) shows the null depth according to the magnitude ratio of the two antennas, and the null is the deepest when the magnitude ratio is the same. Therefore, the proposed method tracks the null to calibrate for both magnitude and phase between two antenna elements by having the 180° phase differences as the calibration reference.

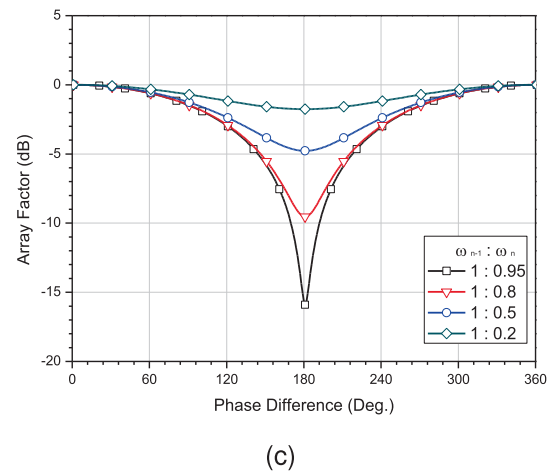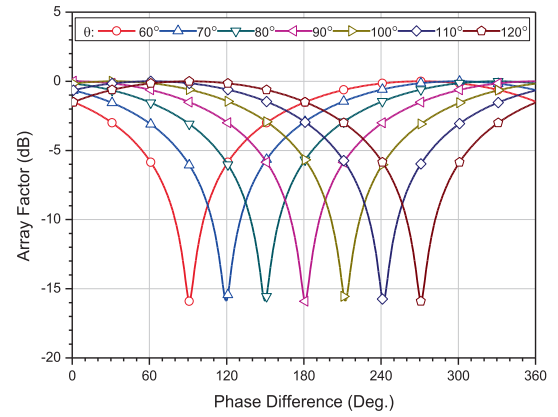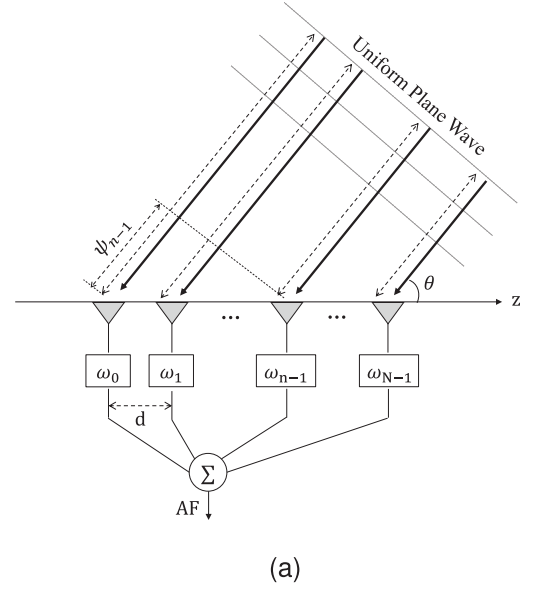(a)

(b)

(c)

Fig. 3 (a) Diagram of the PAA for array factor with N weights. Array factor with regard to phase difference of two antennas with (b) null location by incident angle and (c) null depth by magnitude ratio when $\theta = 90°$.
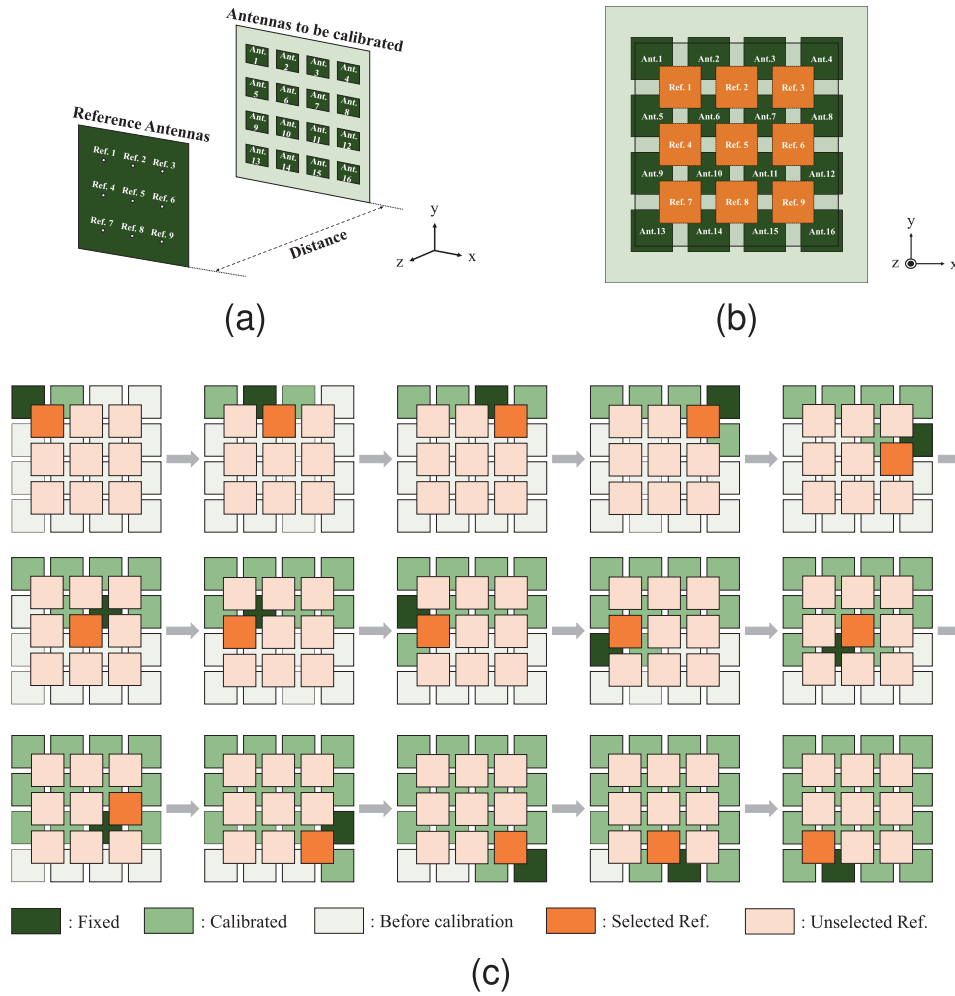
Fig. 4 (a) Simulation environment for the calibration and (b) x-y plane view. (c) Calibration sequence with a horizontal scanning direction.

2.2. Simulation of proposed method

In this subsection, an exemplary calibration scenario is simulated to describe the proposed method. The reference antenna and the array antenna to be calibrated are distant from each other in the far-field region as shown in Fig. 4 (a). The antennas to be calibrated and reference antennas include 4 × 4 and 3 × 3 arrangements, respectively. The antenna elements in the 3x3 reference array are aligned toward the middle of the four corresponding antenna elements to be calibrated to accurately detect nulls as shown in Fig. 4 (b). The simulation proceeds by monitoring the transmission parameters (S_{21}) with regards to the phase difference of two calibration elements, where it has a resolution of 1°. Fig. 4 (c) shows the exemplary calibration sequence in the horizontal scanning direction which is the most basic sequence. Although there might be other faster calibration sequences like starting from the middle elements or scanning diagonally, the horizontal scanning sequence is chosen because it is the simplest algorithm. More importantly, this paper is rather focused on verifying the new calibration hardware and method instead of optimizing the scanning time. In Fig. 4 (c), "fixed", "calibrated", "before calibration", "selected reference", and "unselected reference" denote the antennas for which magnitude and phase are referenced, the target antenna for calibration, the uncalibrated antenna, the reference antenna selected to find the correct null, and the unselected reference antenna, respectively. In the first step, antenna 1 (green square) and antenna 2 (light green square) are calibrated through reference 1 (orange square) using the proposed method. In the second step, antenna 2 and antenna 3 are calibrated through reference 2. This method continues until the last sequence. Once an initially selected two elements are compared and calibrated, one of the two element remains as the reference element to compare the next element. By doing so, the phase variation among the phase shifters due to intrinsic nature of active component can be also minimized.
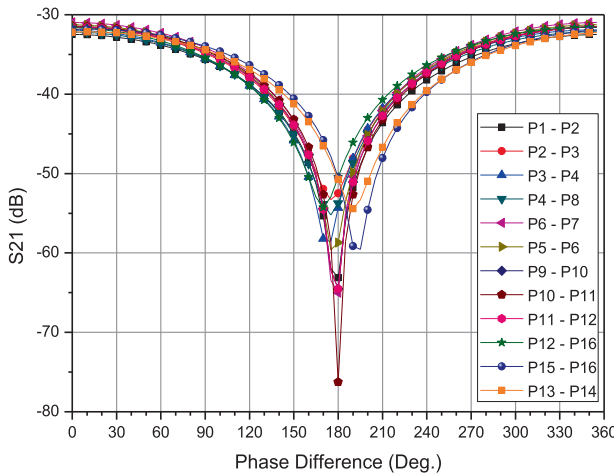
Fig. 5 shows the simulated transmission characteristics of the proposed 4 × 4 array. The free-space path loss of the proposed method and the conventional REV are simulated according to the phase imbalance between antenna 1 and
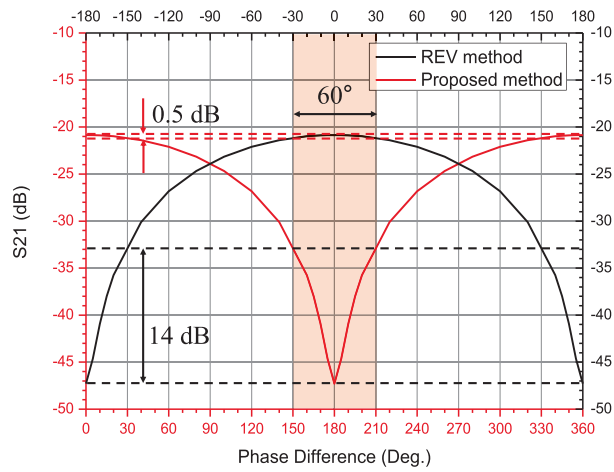
(a)
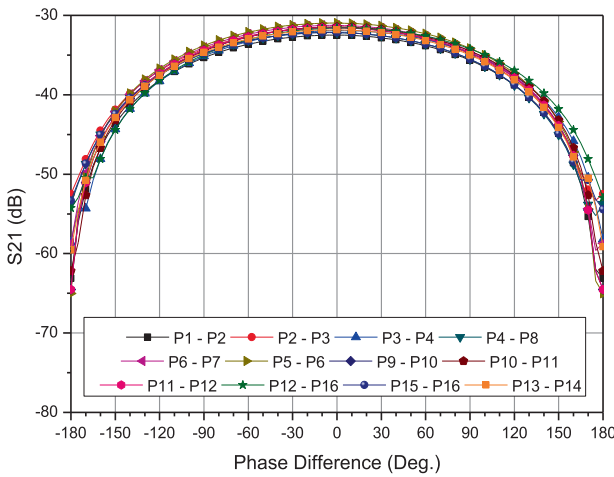
(b)

(c)

Fig. 5 Simulation results of calibration with (a) each S_{21} by phase difference of antenna 1 and antenna 2 after the REV calibration and the proposed calibration. (b) the REV calibration and (c) the proposed calibration results of all elements in an array at 5.8 GHz.

antenna 2 as shown in Fig. 5 (a). The dynamic range of the calibration magnitude by the proposed method over the 60° phase around the null is about 14 dB, whereas the conventional REV shows a dynamic range of 0.5 dB around the maximum point. According to the simulation, the proposed method shows a 13.5 dB higher resolution than the REV method. Since the conventional REV has very small changes in S_{21} per change in phase near the maximum point, a small variation in phase cannot be distinguished accurately based on the magnitude-based method. However, the proposed method has a better detectable resolution in terms of the distinct magnitude level changes per small phase variation. That is, the proposed method can significantly improve the calibration accuracy by
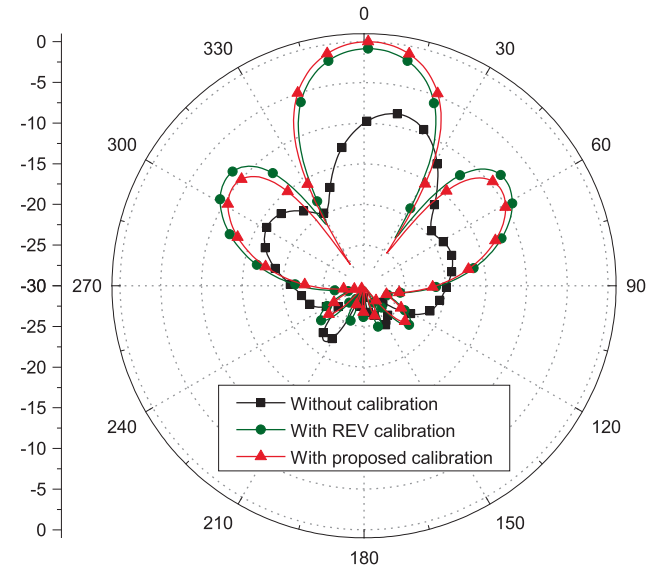
(a)
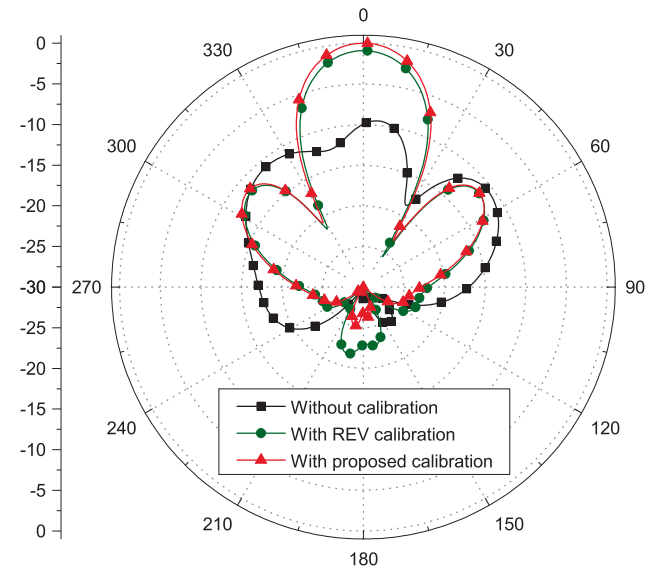
(b)

Fig. 6 Comparative simulated results of normalized radiation patterns after the REV and proposed calibration in (a) E-plane and (b) H-plane at 5.8 GHz.

monitoring only the magnitude behavior in the far-field calibration. Further, since only an RF power detector is required to monitor the received power for vector calibration, the system complexity can be drastically lowered. Then, Fig. 5 (b) and Fig. 5 (c) show the REV calibration and proposed calibration results for all elements in the 4 × 4 array initially having the random phase variation among elements. Also, the simulated radiation patterns of the 4 × 4 array with and without calibration are presented in Fig. 6. The simulated peak gain in E-plane is improved by 9.85 dB and 0.85 dB, respectively, than without calibration and REV calibration, showing that the proposed method in PAA has better performance than the REV method. In H-plane, the simulated peak gain is improved by 9.95 dB and 0.91 dB than without calibration and REV calibration, respectively. An improvement by the proposed calibration with high accuracy will reduce the number of arrays, or broaden device selection and provide a higher signal-to-noise ratio (SNR). As an example in the practical case, [30] designed 256 elements as a satellite transmitter. If

the magnitude is increased by 0.85 dB using the proposed method instead of the conventional REV method, it has the effect of reducing 45 elements while maintaining the same performance. This effect is greatly exerted in larger-scale PAAs.

3. Proposed calibration system design

The system design was carried out to validate the proposed calibration method. Fig. 7 (a) shows the overall system diagram, including a pilot signal generation and received power detection T/Rx board, reconfigurable switch matrix, 16-channel beamformer, 4 × 4 array antenna for calibration, 3 × 3 reference antenna, and switching board to control the reference antenna array. Each block will be discussed in the following individual subsections. Also, a software graphical user interface (GUI) for automatic calibration control was implemented by MATLAB and the Arduino microcontroller. Then, both phase and magnitude deviations in the array was measured and calibrated by different methods such as vector network

(a)

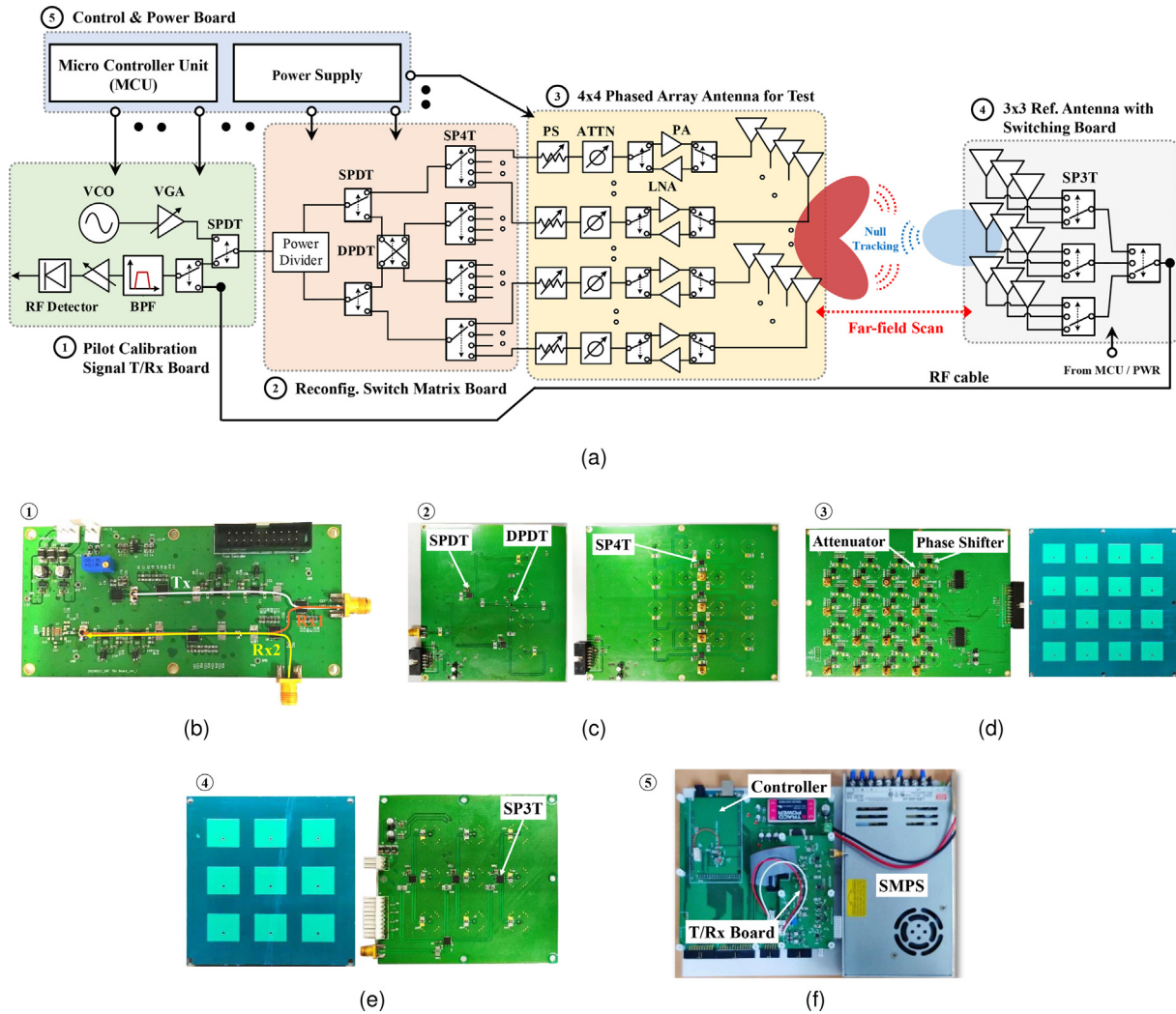(b)   (c)   (d)

(e)   (f)

Fig. 7 (a) Auto-calibration system diagram for proposed method, REV, and non-calibration. Implemented board of (b) pilot calibration signal T/Rx, (c) reconfigurable switch matrix, (d) 4 × 4 phased array antenna for test, (e) 3 × 3 reference antenna with switching circuit, (f) control and power.

analyzer (VNA), auto-calibration based on the proposed method, and the REV for accuracy comparison.

### 3.1. Pilot Signal T/Rx Board Design

Fig. 7 (b) shows the implemented pilot signal T/Rx board where a calibration pilot signal is generated and received power from the reference antenna is detected. Specifically, the transmitter generates an RF signal through the voltage-controlled oscillator (VCO) and controls output gains through a variable gain amplifier (VGA). Also, the single-pole-double-throw (SPDT) RF switch is used to switch and calibrate the array antenna either in the transmission mode or reception mode. The Tx port of the pilot signal T/Rx board is connected to the following reconfigurable switch matrix. Also, the Rx port is connected to the reference antenna switching board to track the null magnitude. The received power is first band-pass filtered to reject interferences and optionally amplified by the VGA to compensate for the RF cable losses and satisfy the dynamic range of the power detector. In other words, By using an RF power detector that can sufficiently detect the minimum power, the dynamic range to be received at the measurement distance is satisfied. The output voltage of the power detector is then connected to the microcontroller unit (MCU) for identifying the optimal calibration point and moving to the next antenna elements.

3.2. Reconfigurable switch matrix board design

Since any two antenna elements could be selected for complete and flexible calibration, a 1:2 reconfigurable switch operation circuit was designed for the whole 16 antenna elements in the exemplary 4×4 PAA as shown in Fig. 7 (c). The switch matrix board is configured by a Wilkinson divider, two SPDT RF switches, one double-pole-double-throw (DPDT) RF switch, and four single-pole-4-throw (SP4T). The divider first divides the pilot signal into two signal paths and each signal path can be connected to any one of the four SP4T switches based on the path control by the two SPDTs and one DPDT. Then, each SP4T can connect the divided pilot signal to any one of the 16 antenna elements with beamforming chains.

3.3. 4×4 Phased array antenna

Fig. 7 (d) shows the implemented 16-channel phased array beamformer and 4×4 patch antenna array at 5.8 GHz. The beamformer board controls the phase and magnitude of each RF chain in the PAA. Each chain consists of a 6-bit phase shifter with 5.6° resolution, and a 6-bit attenuator with 0.5 dB resolution. Since the preceding switch matrix can select any two RF chains, any pair of antenna elements can be compared with the 180° phase difference by adjusting the phase shifters in the
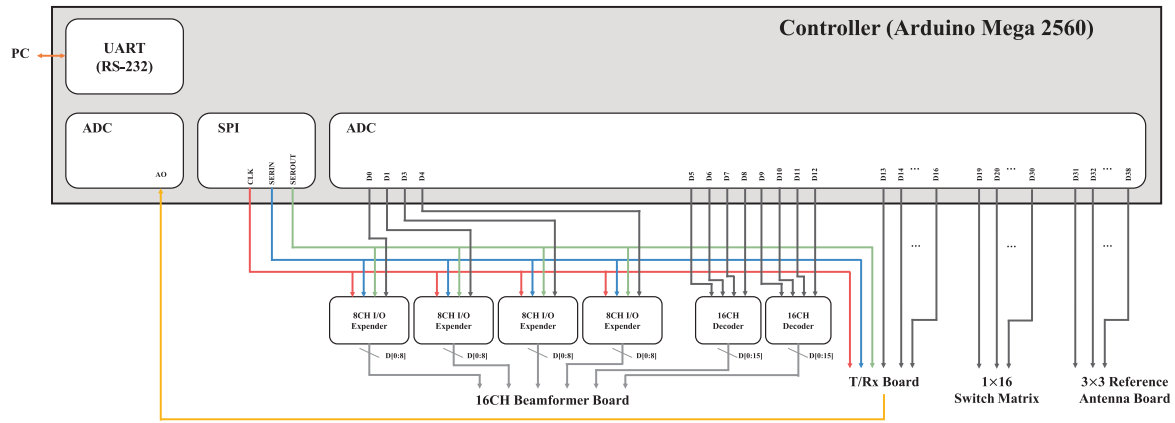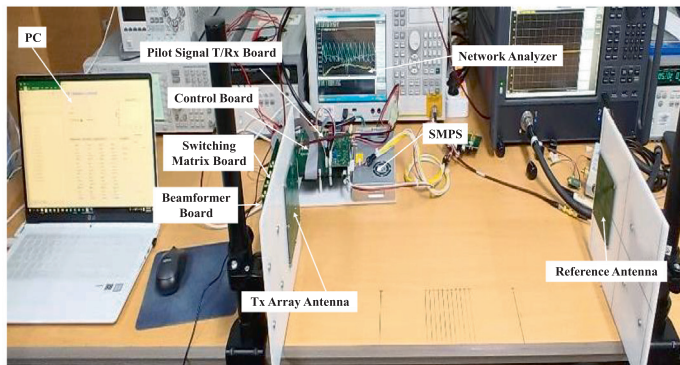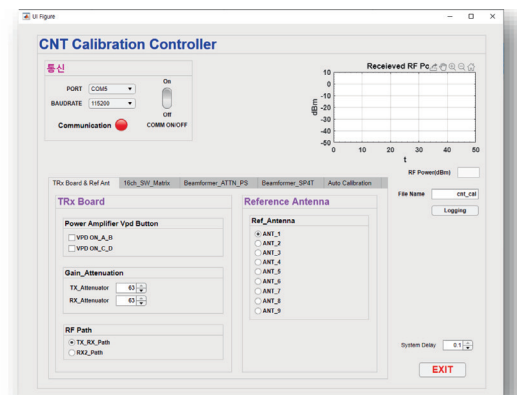
Fig. 8 (a) Control system design for calibration with control block diagram, (b) measurement environment and (c) GUI.

beamformer. Having the 180° phase difference as the ideal calibration reference, the phase and magnitude variation from the reference will be the values to be compensated for calibration. The proposed method purely varies the phase shifter so that it is an opposite phase or 180° phase difference for minimum power. If there is a phase difference from the first 180° at the actual minimum power, since it is an actual phase difference between antennas, calibration is performed to obtain the maximum power by compensating for the phase difference.

3.4. Reference antenna switching board and array antenna design

Fig. 7 (e) shows the implemented 3 × 3 reference antenna with a 1:9 switching circuit. The switching circuit was configured by four single-pole-3-throw (SP3T) to change the reference antenna to be in the proper far-field line-of-sight (LoS) depending on the antenna elements in the PAA under calibration. That is, one of 9 possible reference antennas can be selected for the 4 × 4 array calibration. If the N × N antenna array were to be calibrated, then N-1 × N-1 reference array would have been designed for the calibration.

3.5. MCU and power supply

Lastly, the MCU for auto-calibration of the proposed method is designed as shown in Fig. 7 (f). The controller which is Arduino Mega 2560 performs switch control and serial peripheral interface (SPI) communication selection control of calibration system boards. In addition, the output voltage of the

RF power detector is read by the MCU. More details are described in the following section. For the operation of the auto-calibration system, the switching mode power supply (SMPS) supplies 24 V power.

4. Measurement

In this section, the phase and magnitude of the 4 × 4 PAA are calibrated using the proposed calibration system implemented in Section 3. Then, the proposed system is to be compared with different calibration schemes such as manual calibration using a vector network analyzer (VNA) and the conventional REV. To efficiently control the proposed calibration system, Arduino Mega 2560-based controller for auto-calibration was designed. Fig. 8 (a) shows the selected control block mapping diagram. The switch control and SPI communication of the proposed calibration system were performed using the digital I/O interfaces. The SPI communication was used to control the digital phase shifters and attenuators, while the output voltage of the RF power detector was read through the analog-to-digital converter (ADC). The test configuration is shown in Fig. 8 (b), where the distance between the PAA under calibration and the reference antenna was 700 mm satisfying far-field at 5.8 GHz. Further, the entire calibration system was controlled through the designed GUI as shown in Fig. 8 (c) through the UART function. Fig. 9 shows the calibration algorithm based on the horizontal scanning sequence used in the measurement.

Two antenna elements in the PAA under calibration and one antenna element in the reference antennas were selected
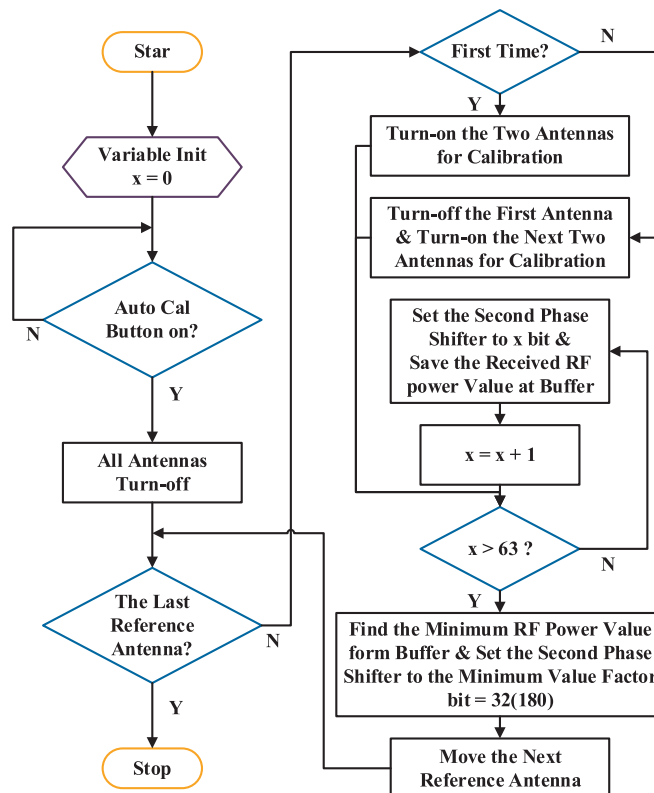

Fig. 9   Algorithm of horizontal scanning direction for proposed auto-calibration.

for calibration. The pilot signal T/Rx board generated the test signal for any two antenna elements in the PAA through the reconfigurable 16-channel switching matrix. Thus, 1×2 antenna radiation could be made by the two antenna elements in the PAA. Next, the received RF power from the far-field radiation to the reference antenna was fed to the pilot signal T/Rx board. The RF power detector converted the power to voltage and the values were stored in the buffer of the MCU while varying the phase of the one antenna element in the PAA from 0° to 360°. Then, the minimum value could be found in the buffer, and the corresponding values were set into the phase shifter and attenuators in the RF chains. The REV method can also be available by finding the maximum value. This cycle continued for the whole antenna element in the PAA until the calibration sequence with the horizontal scanning direction was completed. Finally, each antenna element was set with the optimal magnitude and phase by adjusting the phase shifter and attenuator in the corresponding RF chain.

Fig. 10 (a) shows the measurement results of the proposed method in comparison with the conventional REV method. It is noted that the conventional method could be also conducted by the proposed calibration system tacking the maximum magnitude instead. According to the measured results, the received magnitude dynamic range within the 60° phases of the proposed and REV methods was approximately 22 dB and 1 dB, respectively. That is, higher calibration resolution and accuracy could be possible with the proposed system because the small phase deviation could be clearly detected by observing the distinct magnitude variation. Then, Fig. 10 (b) shows the complete result after processing the proposed calibration for the 4×4 PAA. All element pairs were calibrated with respect to the null. Further, the calibration accuracy was analyzed by comparing the proposed method with the REV method. Fig. 10 (c) shows the measured result of the calibrations. The proposed calibration shows a maximum deviation of 9.89° while the REV calibrations show a maximum deviation of 54°. Thus, an outstanding calibration could be observed by the proposed technique where the phase deviation of each element was closest to 0° after the proposed calibration. As a result, the measured peak gain in E-plane is improved by 9.28 dB and 0.87 dB as shown in Fig. 11, respectively, than without calibration and REV calibration, showing that the proposed method in PAA has better performance than the REV method. In H-plane, the simulated peak gain is improved by 9.46 dB and 0.76 dB than without calibration and REV calibration, respectively. In addition, after REV correction, the beams were tilted by 3° and 4° occurred in the E-plane and H-plane, respectively.

Both the conventional REV method and the proposed method use a phase shifter with a finite resolution, which causes quantization error. The quantization error of the proposed method is affected by the bit of the phase shifter because the maximum quantization error is half the phase shifter resolution [31]. Larger errors do not occur by using different states of the phase shifter. For example, the maximum errors of a 4-bit phase shifter are no bigger than 11.25°. By the same principle, a 6-bit phase shifter has a maximum error of 2.81°. In this paper, a 6-bit phase shifter is selected and includes an error of up to 2.81°. The same goes for the conventional REV method.
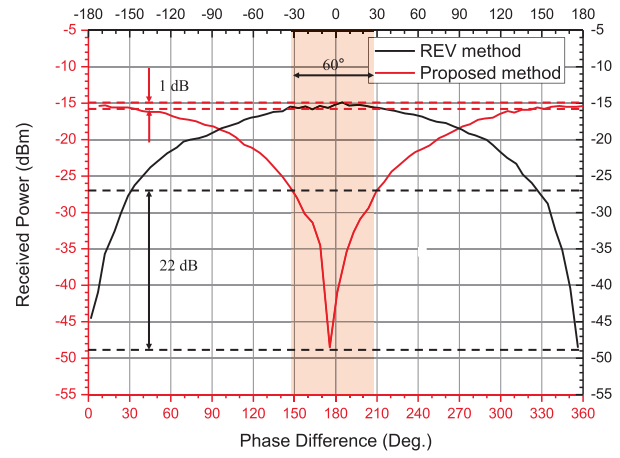
(a)
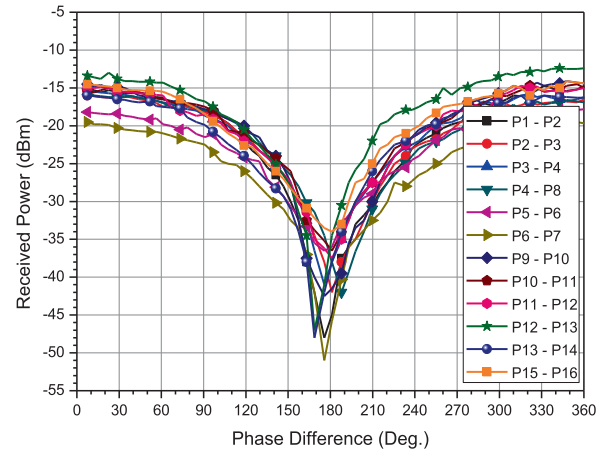
(b)
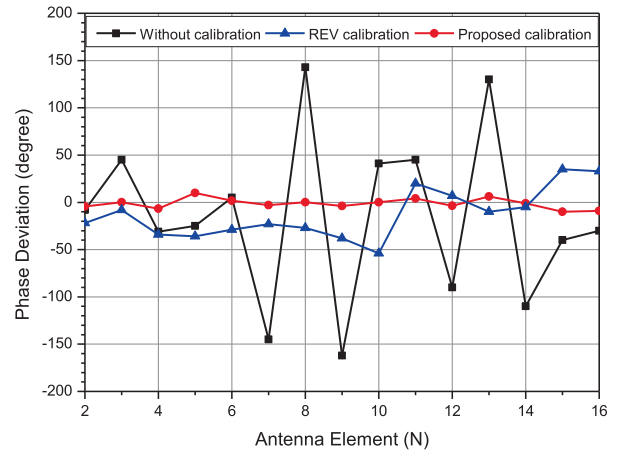
(c)

Fig. 10 Measurement results with (a) each received power with regard to phase difference of antenna 1 and antenna 2 after proposed calibration and REV calibration, and (b) proposed calibration results of all elements in 4×4 array at 5.8 GHz. (c) Phase deviation of each calibration results.
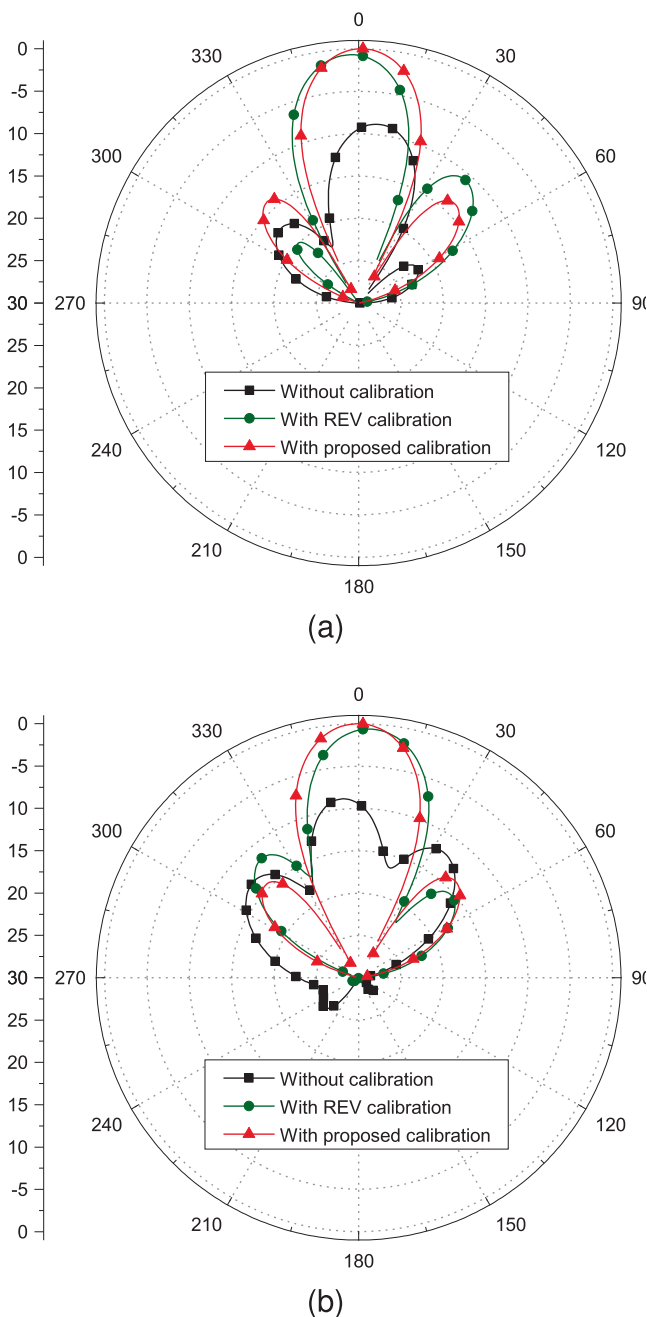
(a)

(b)

Fig. 11 Comparative measured results of normalized radiation patterns after the REV and proposed calibration in (a) E-plane and (b) H-plane at 5.8 GHz.

(a)

(b)

Fig. 12 The received power with (a) proposed method and (b) REV method. Arrows are the recognized values by system per number of tries.

For factory calibration to generate reference LUT, yield is a very important factor for which the accuracy per number of tries should maintain high. Thus, to verify the yield of the proposed method, 10 trials of the proposed calibration and the REV were conducted and denoted by the arrows in Fig. 12. The error ranges of the proposed calibration and the REV method were 5.57° and 59.15°, respectively. That is, the error range of the proposed method was reduced to 0.094 times compared to the REV method, showing the excellent performance of the proposed calibration with a very low-complexity system. Even when the power detector receives a power lower than the
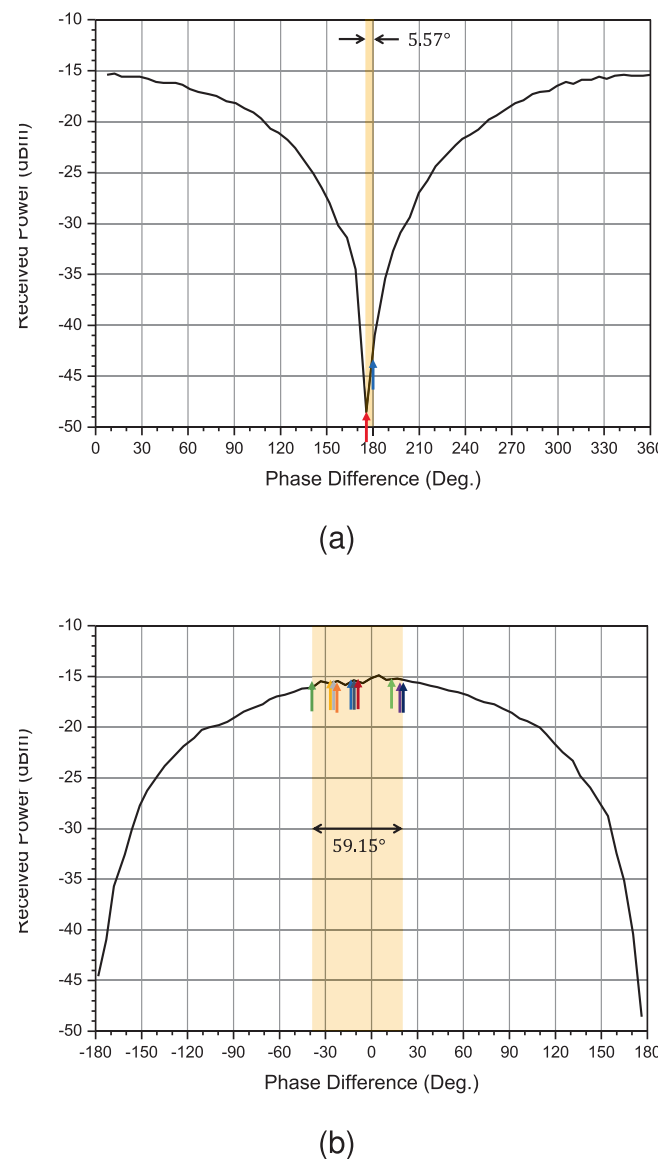
minimum detection power, the proposed method can be used because the minimum power change with amplitude and phase can be observed. In addition, if the minimum detection power of the power detector has a lower minimum detection power, the phase error of the proposed method can be further reduced.

5. Conclusion

This paper proposed the new far-field calibration system that could efficiently improve both accuracy and system complexity. The proposed method was distinguished from the existing far-field-based solutions by tracking the null magnitude of two vector-sum elements in the array while the conventional REV-based methods tracked the maximum magnitude. Then, the

proposed method was verified by implementing a 4×4 calibration system at 5.8 GHz and compared with the conventional REV method. The proposed method showed a better detection range per phase change corresponding to a 22 dB higher resolution. Further, the proposed method showed the phase deviation among the antenna elements within 9.89° whereas the REV method showed the maximum phase deviation of 54°. Lastly, to verify the reliability of the proposed system, a total of 10 trials were repeated. The deviation of the proposed system among each trial was 5.57° whereas the REV method showed 59.15°. Thus, the proposed method can be considered the efficient solution for a large-scale phased array calibration system at the factory level to produce initial LUT.

Declaration of Competing Interest

The authors declare that they have no known competing financial interests or personal relationships that could have appeared to influence the work reported in this paper.

Acknowledgments

References

[1] M.J. Pamies Porras, T. Bertuch, C. Loecker, R. Adams, R. Wunderlich, S. Heinen, An AESA antenna comprising an RF feeding network with strongly coupled antenna ports, IEEE Trans. Antennas Propag. 63 (1) (2015) 182–194, Jan..

[2] S. Lim, I. Choi, T. Jeong, Compensation Method for a Wideband Signal's Squint Problem of an AESA SAR System Using a Cross-Range-Variant Antenna Gain Equalizer, IEEE Sens. J., vol. 19, no. 8, pp. 2937–2945, 15 April 15, 2019.

[3] J.S. Herd, M.D. Conway, The evolution to modern phased array architectures, Proc. IEEE 104 (3) (2016) 519–529, March.

[4] G.H.C. Van Werkhaven, A.K. Golshayan, Calibration aspects of the APAR antenna unit, Proceedings 2000 IEEE Int. Conf. on Phased Array Systems and Technology (Cat. No.00TH8510) (2000) 425–428.

[5] J. del Castillo, S. Sánchez, R. de Porras, A. Pedreira, J.R. Larrañaga, L-Band Digital Array Radar Demonstrator for Next Generation Multichannel SAR Systems, IEEE J. Select. Top. Appl. Earth Observ. Remote Sens. 8 (11) (2015) 5007–5014, Nov..

[6] M. Sarcione et al, The design, development and testing of the THAAD (Theater High Altitude Area Defense) solid state phased array (formerly ground based radar), Proc. Int. Symp. on Phased Array Systems and Technology (1996) 260–265.

[7] S.M. Moon, S. Yun, I.B. Yom, H.L. Lee, Phased Array Shaped-Beam Satellite Antenna With Boosted-Beam Control, IEEE Trans. on Antennas and Propag. 67 (12) (2019) 7633–7636, Dec..

[8] J.M. Fernandez Gonzalez, P. Padilla, G. Exposito-Dominguez, M. Sierra-Castaner, Lightweight Portable Planar Slot Array Antenna for Satellite Communications in X-Band, IEEE Antennas and Wireless Propag. Letters 10 (2011) 1409–1412.

[9] K. Gulur Sadananda, M.P. Abegaonkar and S.K. Koul, Gain Equalized Shared-Aperture Antenna Using Dual-Polarized ZIM for mmWave 5G Base Stations, IEEE Antennas and Wireless Propag. Letters, vol. 18, no. 6, pp. 1100–1104, June 2019.

[10] H. Hu, F. Lai, Y. Chen, Dual-Band Dual-Polarized Scalable Antenna Subarray for Compact Millimeter-Wave 5G Base Stations, IEEE Access 8 (2020) 129180–129192.

[11] M.S.F. Reyhan, Y. Rahayu, F. Muhammadsyah, The Design of Broadband 8x2 Phased Array 5G Antenna MIMO 28 GHz for Base Station, World Academy of Science, Engineering and Technology Int, Journal of Electronics and Communication Engineering 12 (2018) 840–843.

[12] D. Muirhead, M.A. Imran, K. Arshad, A Survey of the Challenges, Opportunities and Use of Multiple Antennas in Current and Future 5G Small Cell Base Stations, IEEE Access 4 (2016) 2952–2964.

[13] C. Fulton, M. Yeary, D. Thompson, J. Lake, A. Mitchell, Digital Phased Arrays: Challenges and Opportunities, Proc. IEEE 104 (3) (2016) 487–503, March.

[14] C. Fulton et al, Cylindrical polarimetric phased array radar: Beamforming and calibration for weather applications, IEEE Trans. Geosci. and Remote Sens. 55 (5) (2017) 2827–2841, May.

[15] I. Seker, Calibration methods for phased array radars, Proc. of SPIE, vol. 8714, 2013.

[16] S.C. Chae, H.W. Jo, J.I. Oh, G. Kim, J.W. Yu, Coupler Integrated Microstrip Patch Linear Phased Array for Self-Calibration, IEEE Antennas and Wireless Propag. Letters 19 (9) (2020) 1615–1619, Sept..

[17] M. Scott, SAMPSON MFR active phased array antenna, IEEE Int. Symp. on Phased Array Systems and Technology (2003) 119–123.

[18] H. Steyskal, J.S. Herd, Mutual coupling compensation in small array antennas, IEEE Trans. on Antennas and Propag. 38 (12) (1990) 1971–1975, Dec..

[19] C. Shipley and D. Woods, Mutual coupling-based calibration of phased array antennas, Proc. 2000 IEEE Int. Conf. on Phased Array Systems and Technology (Cat. No.00TH8510), 2000, pp. 529–532.

[20] H.M. Aumann, A.J. Fenn, F.G. Willwerth, Phased array antenna calibration and pattern prediction using mutual coupling measurements, IEEE Trans. on Antennas and Propag. 37 (7) (1989) 844–850.

[21] A. Agrawal, A. Jablon, A calibration technique for active phased array antennas, IEEE Int, Symp. on Phased Array Systems and Technology (2003) 223–228.

[22] A. Nafe, K. Kibaroglu, M. Sayginer, G.M. Rebeiz, An In-Situ Self-Test and Self-Calibration Technique Utilizing Antenna Mutual Coupling for 5G Multi-Beam TRX Phased Arrays, 2019 IEEE MTT-S Int. Microw. Symp. (IMS) (2019) 1229–1232.

[23] S. Mano, T. Katagi, A Method for Measuring Amplitude and Phase of Each Radiating Element of a Phased Array Antenna, Electronics and Communications in Japan (1982) 58–64.

[24] A.M. Shitikov, A.V. Bondarik, Multi-element PAA calibration with REV method, 4th Int, Conf. on Antenna Theory and Techniques (Cat. No.03EX699) (2003) 761–764.

[25] B. Wang, Y.L.M. Gao, B. Tian, A new combined rotatingelement electric-field vector(REV) calibration method for large phased array antenna, 2017 Int. Applied Computational Electromagnetics Society Symp. (ACES) (2017).

[26] B. Wang, Y. Li, B. Tian, Rotating-element electric-field vector (REV) calibration method based on power measurement for phased array antenna, 2017 Int. Applied Computational Electromagnetics Society Symp. (ACES) (2017).

[27] H.-J. Yoon, B.-W. Min, Improved Rotating-Element Electric-Field Vector Method for Fast Far-Field Phased Array Calibration, IEEE Trans. on Antennas and Propag. 69 (11) (2021) 8021–8026, Nov..

[28] T. Takahashi, Y. Konishi, S. Makino, H. Ohmine, H. Nakaguro, Fast Measurement Technique for Phased Array Calibration, IEEE Trans. on Antennas and Propag. 56 (7) (2008) 1888–1899, July.

[29] M. Liu, Z. Feng, Combined Rotating-element Electric-field Vector (CREV) Method for nearfield Calibration of Phased Array Antenna, 2007 Int, Conf. on Microw. and Millim. Wave Technol. (2007) 1–4.

[30] A.H. Aljuhani, T. Kanar, S. Zihir and G.M. Rebeiz, A 256-Element Ku-Band Polarization Agile SATCOM Transmit Phased Array With Wide-Scan Angles, Low Cross Polarization, Deep Nulls, and 36.5-dBW EIRP per Polarization, IEEE Trans. Microwave Theory Tech., vol. 69, no. 5, pp. 2594–2608, May 2021.

[31] B. Wang, Yan Li, B. Tian, Rotating-element electric-field vector (REV) calibration method based on power measurement for phased array antenna, in: 2017 International Applied Computational Electromagnetics Society Symposium (ACES), 2017, pp. 1–2.